J|A|C|S ARTICLES

Published on Web 03/23/2009

Free Energy Landscapes for S−H Bonds in $Cp^*_2Mo_2S_4$ Complexes

Aaron M. Appel, Suh-Jane Lee, James A. Franz,* Daniel L. DuBois, and M. Rakowski DuBois

Pacific Northwest National Laboratory, P.O. Box 999, Richland, Washington 99352

Received November 28, 2008; E-mail: james.franz@pnl.gov

Abstract: An extensive family of thermochemical data is presented for a series of complexes derived from $Cp^*Mo(\mu\text{-}S)_2(\mu\text{-}SMe)(\mu\text{-}SH)MoCp^*$ and $Cp^*Mo(\mu\text{-}S)_2(\mu\text{-}SH)_2MoCp^*$. These data include electrochemical potentials, pK_a values, homolytic solution bond dissociation free energies (SBDFEs), and hydride donor abilities in acetonitrile. Thermochemical data ranged from +0.6 to −2.0 V vs $FeCp_2^{+/o}$ for electrochemical potentials, 5 to 31 for pK_a values, 43 to 68 kcal/mol for homolytic SBDFEs, and 44 to 84 kcal/mol for hydride donor abilities. The observed values for these thermodynamic parameters are comparable to those of many transition metal hydrides, which is consistent with the many parallels in the chemistry of these two classes of compounds. The extensive set of thermochemical data is presented in free energy landscapes as a useful approach to visualizing and understanding the relative stabilities of all of the species under varying conditions of pH and H_2 overpressure. In addition to the previously studied homogeneous reactivity and catalysis, Mo_2S_4 complexes are also models for heterogeneous molybdenum sulfide catalysts, and therefore, the present results demonstrate the dramatic range of S−H bond strengths available in both homogeneous and heterogeneous reaction pathways.

Introduction

Homogeneous Mo_2S_4 complexes have been widely studied as a result of the prevalence of molybdenum sulfides in both hydrogenation and hydrodesulfurization (HDS)[1−3] catalysts and enzymes.[3−5] Investigations of these homogeneous Mo_2S_4 complexes cover a broad range of topics, including catalysis and electrocatalysis,[6−11] a wide variety of bond forming reactions,[12−19] free radical reactivity,[20−24] photolytic reactions,[25] and the preparation of heterometallic sulfide clusters.[26−31] In spite of the importance of molybdenum sulfide chemistry and the extensive research into Mo_2S_4 complexes, very few S−H bond energies have been determined for MoS−H bonds,[6,32] even though they are key to a fundamental understanding of

(1) Grange, P.; Vanhaeren, X. *Catal. Today* **1997**, *36*, 375–391.
(2) Bianchini, C.; Meli, A. *Acc. Chem. Res.* **1998**, *31*, 109–116.
(3) Donahue, J. P. *Chem. Rev.* **2006**, *106*, 4747–4783.
(4) Hille, R. *Chem. Rev.* **1996**, *96*, 2757–2816.
(5) Brondino, C. D.; Rivas, M. G.; Romao, M. J.; Moura, J. J. G.; Moura, I. *Acc. Chem. Res.* **2006**, *39*, 788–796.
(6) Appel, A. M.; DuBois, D. L.; Rakowski DuBois, M. *J. Am. Chem. Soc.* **2005**, *127*, 12717–12726.
(7) Rakowski DuBois, M. In *Catalysis by Di- and Polynuclear Metal Cluster Complexes*; Adams, R. D., Cotton, F. A., Eds.; Wiley-VCH: New York, 1998; pp 127−143.
(8) Rakowski DuBois, M. *Chem. Rev.* **1989**, *89*, 1–9.
(9) Casewit, C. J.; Coons, D. E.; Wright, L. L.; Miller, W. K.; Rakowski DuBois, M. *Organometallics* **1986**, *5*, 951–955.
(10) Kubas, G. J.; Ryan, R. R. *J. Am. Chem. Soc.* **1985**, *107*, 6138–6140.
(11) Rakowski DuBois, M.; Haltiwanger, R. C.; Miller, D. J.; Glatzmaier, G. *J. Am. Chem. Soc.* **1979**, *101*, 5245–5252.
(12) Kubas, G. J.; Ryan, R. R.; Kubatmartin, K. A. *J. Am. Chem. Soc.* **1989**, *111*, 7823–7832.
(13) Rakowski DuBois, M.; Vanderveer, M. C.; DuBois, D. L.; Haltiwanger, R. C.; Miller, W. K. *J. Am. Chem. Soc.* **1980**, *102*, 7456–7461.
(14) Bernatis, P.; Laurie, J. C. V.; Rakowski DuBois, M. *Organometallics* **1990**, *9*, 1607–1617.
(15) Newell, R.; Ohman, C.; Rakowski DuBois, M. *Organometallics* **2005**, *24*, 4406–4415.
(16) Rakowski DuBois, M.; Vasquez, L. D.; Ciancanelli, R. F.; Noll, B. C. *Organometallics* **2000**, *19*, 3507–3515.
(17) Farmer, M. M.; Haltiwanger, R. C.; Kvietok, F.; Rakowski DuBois, M. *Organometallics* **1991**, *10*, 4066–4070.
(18) Brunner, H.; Meier, W.; Wachter, J.; Weber, P.; Ziegler, M. L.; Enemark, J. H.; Young, C. G. *J. Organomet. Chem.* **1986**, *309*, 313–318.
(19) Brunner, H.; Kauermann, H.; Meier, W.; Wachter, J. *J. Organomet. Chem.* **1984**, *263*, 183–192.
(20) Casewit, C. J.; Haltiwanger, R. C.; Noordik, J.; Rakowski DuBois, M. *Organometallics* **1985**, *4*, 119–129.
(21) Casewit, C. J.; Rakowski DuBois, M. *J. Am. Chem. Soc.* **1986**, *108*, 5482–5489.
(22) Birnbaum, J.; Godziela, G.; Maciejewski, M.; Tonker, T. L.; Haltiwanger, R. C.; Rakowski DuBois, M. *Organometallics* **1990**, *9*, 394–401.
(23) Franz, J. A.; Birnbaum, J. C.; Kolwaite, D. S.; Linehan, J. C.; Camaioni, D. M.; Dupuis, M. *J. Am. Chem. Soc.* **2004**, *126*, 6680–6691.
(24) Appel, A. M.; Lee, S.-J.; Franz, J. A.; DuBois, D. L.; Rakowski DuBois, M.; Birnbaum, J. C.; Twamley, B. *J. Am. Chem. Soc.* **2008**, *130*, 8940–8951.
(25) Bruce, A. E.; Tyler, D. R. *Inorg. Chem.* **1984**, *23*, 3433–3434.
(26) Curtis, M. D.; Williams, P. D. *Inorg. Chem.* **1983**, *22*, 2661–2662.
(27) Curtis, M. D.; Riaz, U.; Curnow, O. J.; Kampf, J. W.; Rheingold, A. L.; Haggerty, B. S. *Organometallics* **1995**, *14*, 5337–5343.
(28) Mansour, M. A.; Curtis, M. D.; Kampf, J. W. *Organometallics* **1997**, *16*, 275–284.
(29) Cowans, B. A.; Haltiwanger, R. C.; Rakowski DuBois, M. *Organometallics* **1987**, *6*, 995–1004.
(30) DuBois, D. L.; Kvietok, F.; Rakowski Dubois, M. *Inorg. Chem.* **1993**, *32*, 561–564.
(31) Brunner, H.; Janietz, N.; Wachter, J.; Zahn, T.; Ziegler, M. L. *Angew. Chem., Int. Ed. Engl.* **1985**, *24*, 133–135.
(32) Appel, A. M.; Lee, S.-J.; Franz, J. A.; DuBois, D. L.; Rakowski DuBois, M.; Twamley, B. *Organometallics*, published on the web 1/12/2009, DOI: 10.1021/om800875n.

10.1021/ja8093179 CCC: $40.75

Chart 1. Structural Representations and Abbreviations of Cp*$_2$Mo$_2$S$_4$ Complexes in This Work (Cp* = η^5-C$_5$Me$_5$)

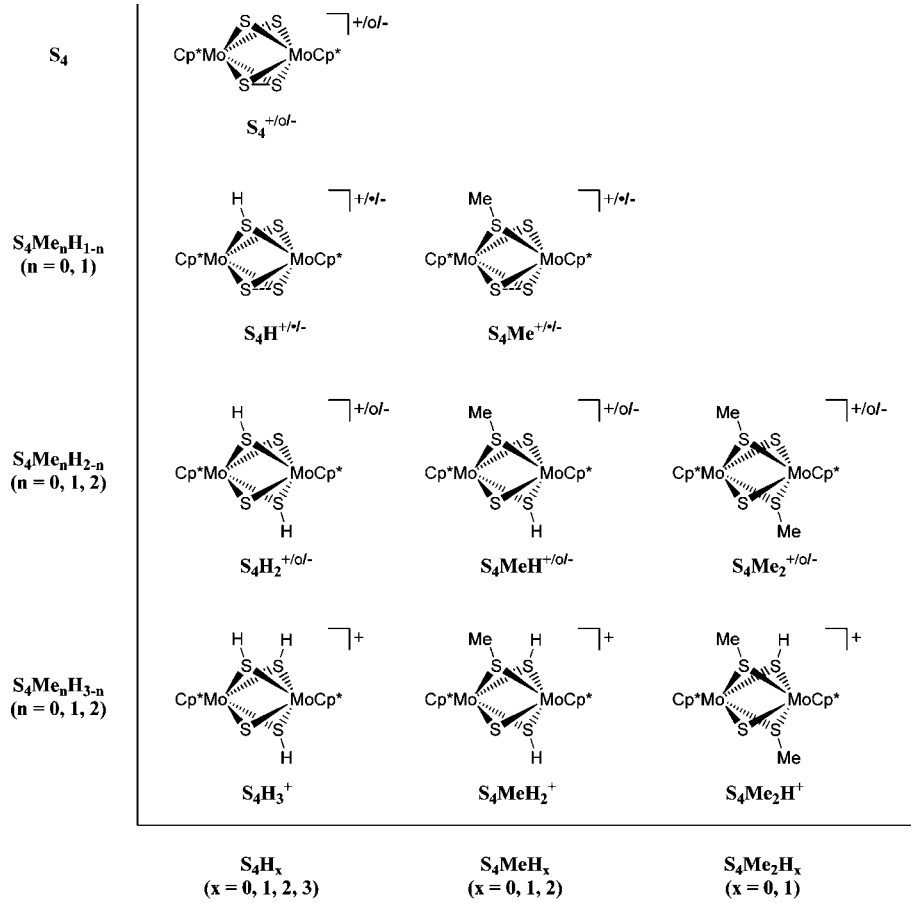

homogeneous and heterogeneous catalysis of hydrogen transfer pathways.

In 2005 we reported the low overpotential of $(CpMoS)_2(S_2CH_2)$ as a proton reduction catalyst and therein the first experimentally determined S−H homolytic solution bond dissociation free energy (SBDFE) in a homogeneous Mo_2S_4 complex.[6] More recently, we reported homolytic SBDFEs for structurally related monoprotonated molybdenum sulfide complexes $[(Cp^*Mo)_2(\mu\text{-}SMe)_2(\mu\text{-}SH)(\mu\text{-}S)]^+$, $[(Cp^*Mo)_2(\mu\text{-}SMe)(\mu\text{-}SH)_2(\mu\text{-}S)]^+$, and $[(Cp^*Mo)_2(\mu\text{-}SH)_3(\mu\text{-}S)]^+$ ($\mathbf{S_4Me_nH_{3-n}}^+$ where $n = 0$, 1, and 2; see Chart 1 for structures and abbreviations).[32]

In these Mo_2S_4 systems all of the reported homolytic SBDFE values were determined for the dissociation of $\mathbf{S_4Me_nH_{3-n}}^+$ to form $\mathbf{S_4Me_nH_{2-n}}^+$ and a hydrogen atom. However, additional S−H bonds are present for $\mathbf{S_4MeH_2}^+$ and $\mathbf{S_4H_3}^+$, and therefore, substantially more extensive thermochemical information can be obtained. The increase in the obtainable data in moving from $\mathbf{S_4Me_2H}^+$ to $\mathbf{S_4MeH_2}^+$ and $\mathbf{S_4H_3}^+$ is similar to the increase in the number of possible bond energies in moving from metal hydrides to metal dihydrides.[33−35]

In this paper we present the determination of additional homolytic SBDFE values, pK_a values, and free energies for hydride transfer for S−H bonds in these soluble molybdenum sulfide complexes. The complexity of this extensively interrelated data presents a challenge for understanding and utilizing the derived thermochemical information. In order to simplify the presentation of these comprehensive data sets, free energy landscapes are introduced in a new approach to illustrate the relative free energies for all the species present under specific conditions.

Results

Determination of Thermochemical Data. The new thermochemical data presented in this work and in previous work on these Mo_2S_4 systems require the measurement of selected pK_a values and a variety of redox potentials. The pK_a values of **S$_4$MeH** and **S$_4$H$_2$** complexes were determined using ^{1}H NMR spectroscopy by measuring the equilibria shown in eq 1 when the base (B) was *tert*-butylimino-tri(pyrrolidino)phosphorane (BTPP, pK_a of conjugate acid = 28.4)[36] or 2,8,9-trimethyl-2,5,8,9-tetraaza-1-phosphabicyclo[3.3.3]undecane (Verkade superbase, pK_a of conjugate acid = 32.9).[37] Each determined value is the average of four or more measurements and includes verification of reversibility. For example, an equilibrium was measured between BTPP and **S$_4$H$_2$**, and then protonated BTPP was added, shifting the equilibrium away from $\mathbf{S_4H}^-$ and back toward **S$_4$H$_2$**. The equilibrium was then remeasured in order to verify that **S$_4$H$_2$** deprotonated reversibly. The equilibrium constants for eq 1 and the known pK_a values[36,37] of the reference acids (BH^+) were used to calculate the pK_a values of **S$_4$MeH**

(33) Ciancanelli, R.; Noll, B. C.; DuBois, D. L.; Rakowski DuBois, M. *J. Am. Chem. Soc.* **2002**, *124*, 2984–2992.
(34) Miedaner, A.; Raebiger, J. W.; Curtis, C. J.; Miller, S. M.; DuBois, D. L. *Organometallics* **2004**, *23*, 2670–2679.
(35) Raebiger, J. W.; DuBois, D. L. *Organometallics* **2005**, *24*, 110–118.
(36) Kaljurand, I.; Kutt, A.; Soovali, L.; Rodima, T.; Maemets, V.; Leito, I.; Koppel, I. A. *J. Org. Chem.* **2005**, *70*, 1019–1028.
(37) Kisanga, P. B.; Verkade, J. G.; Schwesinger, R. *J. Org. Chem.* **2000**, *65*, 5431–5432.

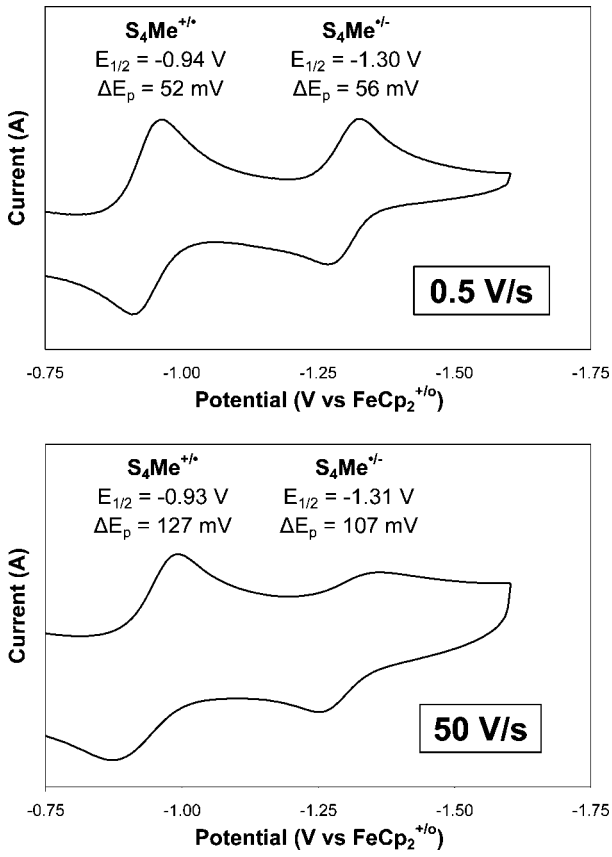

Figure 1. Cyclic voltammograms of 2 mM $\mathbf{S_4Me}^+$ at 0.5 (top) and 50 V/s (bottom), both in 0.3 M NEt_4BF_4 in acetonitrile (the redox couple for the internal reference is not shown). Note the decrease in the cathodic wave at −1.31 V relative to the other waves at 50 V/s.

(31.0 ± 0.6) and $\mathbf{S_4H_2}$ (29.8 ± 0.4) using eq 2 (where B is the base form of the reference, BH^+ is the acid form of the reference, and K_{eq} is the equilibrium constant for eq 1). The estimated errors include contributions from experimental irreproducibility and uncertainties in the pK_a values of the reference acids. The higher pK_a value for the methylated analogue is expected given that a methyl group is a better electron donor than a hydrogen atom, consistent with the results from the previously studied $\mathbf{S_4Me}_n\mathbf{H}_{3-n}^+$ complexes.[32] A pK_a value of 10.4 ± 0.3 was determined for $\mathbf{S_4H}^+$ using a similar approach, and details are given in the Experimental Procedures. Note that in all reported equilibrium studies where multiple structural isomers are possible,[23,24] that the observable isomers typically occur in a ratio of ∼2:1, corresponding to 0.3 kcal/mol. In the cases where isomers are observed, they have been averaged, and the differences in energies between the isomers are well within the reported experimental errors.

$$S_4MeH + B \overset{K_{eq}}{\rightleftharpoons} S_4Me^- + BH^+ \quad (1a)$$

$$S_4H_2 + B \overset{K_{eq}}{\rightleftharpoons} S_4H^- + BH^+ \quad (1b)$$

$$pK_{a\_analyte} = pK_{a\_ref} - \log(K_{eq}) \quad (2)$$

Cyclic voltammetry experiments were used in previous studies of $\mathbf{S_4Me_2}$, $\mathbf{S_4MeH}$, and $\mathbf{S_4H_2}$ to determine the potentials of the $\mathbf{S_4Me}_n\mathbf{H}_{2-n}^{\bullet+/o}$ and $\mathbf{S_4Me}_n\mathbf{H}_{2-n}^{o/\bullet-}$ couples.[32] All potentials are referenced to the ferrocenium/ferrocene couple using ferrocene or decamethylferrocene as an internal standard. Additional cyclic voltammetry experiments have now given potentials for the $\mathbf{S_4Me}^{2+/+/\bullet/-}$, $\mathbf{S_4H}^{+/\bullet/-}$, and $\mathbf{S_4}^{\bullet+/o/\bullet-}$ couples. For $\mathbf{S_4Me}^+$, three apparently reversible electron transfer reactions are observable, corresponding to the $\mathbf{S_4Me}^{2+/+/\bullet/-}$ species. Although the $\mathbf{S_4Me}^{+/\bullet}$ and $\mathbf{S_4Me}^{\bullet/-}$ couples appear to be simple reversible waves at slow scan rates (≤0.5 V/s, as shown in the top of Figure 1), at scan rates of 5 V/s or higher, the current for the cathodic wave at −1.30 V decreases (bottom of Figure 1). A similar decrease is observed for the anodic wave at −0.93 V when starting from $\mathbf{S_4Me}^-$ (formed in situ by deprotonation of **S_4MeH**). Scan-rate-dependent changes in the shape of the voltammogram typically suggests a chemical step that occurs before or after an electron transfer. In this case, the $\mathbf{S_4Me}^\bullet$ radical is known to reversibly dimerize (eq 3) with a rate constant of 6.3×10^7 M^{-1} s^{-1} and dissociate with a rate constant of 1.1×10^3 s^{-1} at 25 °C.[24] Because the dimerization of $\mathbf{S_4Me}^\bullet$ that follows either reduction of $\mathbf{S_4Me}^+$ or oxidation of $\mathbf{S_4Me}^-$ is fast, the oxidation or reduction of the radical monomer, $\mathbf{S_4Me}^\bullet$, must await dissociation of the dimer. This slow dissociation decreases the current observed for either the reduction or oxidation of $\mathbf{S_4Me7}^\bullet$ at scan rates of 5 V/s or higher.

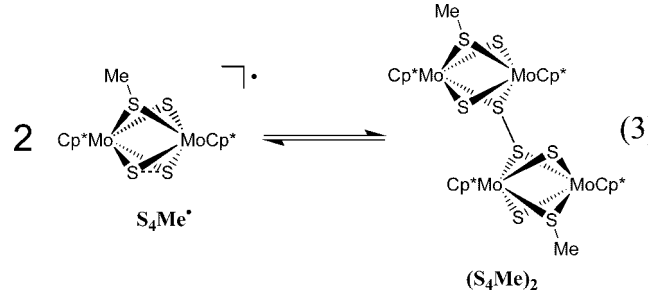

Simulations of the effects of this dimerization upon the potentials for the $\mathbf{S_4Me}^{+/\bullet}$ and $\mathbf{S_4Me}^{\bullet/+}$ couples show that the shift of the observed potentials from the true potentials is expected to be small (≤80 mV), even at a relatively slow scan rate of 0.5 V/s and a high concentration of 6.6 mM (see Supporting Information for details of the simulations). A number of thermodynamic values discussed below depend on the potentials of both the $\mathbf{S_4Me}^{+/\bullet}$ and $\mathbf{S_4Me}^{\bullet/-}$ couples, which are −0.99 ± 0.02 and −1.24 ± 0.03 V, respectively, after correcting for dimerization. It is important to emphasize that any errors in the redox potentials arising from the formation and cleavage of the dimer will not affect thermochemical data that require both potentials. The errors introduced in the individual redox potentials by the following reactions will be equal and opposite and therefore cancel out when both of the couples are used. One example is the hydride donor ability for **S_4MeH** to form $\mathbf{S_4Me}^+$ and H^-, specifically that the pK_a for **S_4MeH** and both the $\mathbf{S_4Me}^{+/\bullet}$ and $\mathbf{S_4Me}^{\bullet/-}$ couples are used. If the potential for the $\mathbf{S_4Me}^{\bullet/-}$ couple is overcorrected, and thereby too positive, the potential for the $\mathbf{S_4Me}^{+/\bullet}$ couple will correspondingly be too negative, resulting in no net change to the hydride donor ability for **S_4MeH**.

The replacement of a methyl group with a hydrogen results in an irreversible oxidation for the $\mathbf{S_4H}^{\bullet/-}$ couple and an irreversible reduction for the $\mathbf{S_4H}^{+/\bullet}$ couple, at all observed scan rates (0.05−50 V/s). The irreversible $\mathbf{S_4H}^{+/\bullet/-}$ couples are the result of disproportionation of $\mathbf{S_4H}^\bullet$ to form $\mathbf{S_4}$ and $\mathbf{S_4H_2}$, as shown in eq 4. Protonation of $\mathbf{S_4}$ and reduction of the generated

Table 1. Cyclic Voltammetry Data for the Mo_2S_4 Complexes in Acetonitrile with 0.3 M NEt_4BF_4

couple	$E_{1/2}$ or E_p[a] (V vs $FeCp_2^{+/o}$)	ΔE_p or $E_p - E_{p/2}$[a] (mV)	scan rate (V/s)
$\mathbf{S_4}^{\bullet+/o}$	−0.17	63	0.05
$\mathbf{S_4}^{o/\bullet-}$	−1.65	71	0.05
$\mathbf{S_4Me}^{2+/+}$	0.64	113	5
$\mathbf{S_4H}^{+/\bullet}$	−0.86[a]	*54*[a]	0.5
$\mathbf{S_4Me}^{+/\bullet}$	−0.93[b]	51	0.05
$\mathbf{S_4H}^{\bullet/-}$	−1.30[a]	*59*[a]	0.5
$\mathbf{S_4Me}^{\bullet/-}$	−1.30[b]	56	0.05
$\mathbf{S_4H_2}^{\bullet+/o}$	0.07[c]	194	200
$\mathbf{S_4MeH}^{\bullet+/o}$	0.04[c]	122	50
$\mathbf{S_4Me_2}^{\bullet+/o}$	−0.02[c]	67	0.5
$\mathbf{S_4H_2}^{o/\bullet-}$	−1.87[c]	63	0.5
$\mathbf{S_4MeH}^{o/\bullet-}$	−1.96[c]	62	0.5
$\mathbf{S_4Me_2}^{o/\bullet-}$	−2.04[c]	67	0.5

[a] E_p is the peak potential, and $E_{p/2}$ is the potential at half-height. $E_{1/2}$ and ΔE_p for all reversible waves, and E_p and $E_p - E_{p/2}$ for irreversible waves, specifically the $\mathbf{S_4H}^{+/\bullet/-}$ couples. [b] $E_{1/2}$ uncorrected for dimerization of $\mathbf{S_4Me}^{\bullet}$. [c] Data for $\mathbf{S_4H_2}^{+/o/-}$, $\mathbf{S_4MeH}^{+/o/-}$, and $\mathbf{S_4Me_2}^{+/o/-}$ from Appel, et al.[32]

$\mathbf{S_4H}^+$ results in the appearance of a wave at −1.87 V, corresponding to formation of $\mathbf{S_4H_2}$. Similarly, deprotonation of $\mathbf{S_4H_2}$ and oxidation of the resulting $\mathbf{S_4H}^-$ produces an oxidation wave at −0.17 V, expected for the formation of $\mathbf{S_4}$, as shown in eq 4.

$$\mathbf{S_4H}^{\bullet} + \mathbf{S_4H}^{\bullet} \rightleftharpoons \mathbf{S_4} + \mathbf{S_4H_2} \qquad (4)$$

In order to estimate $E_{1/2}$ values from these irreversible peak potentials, simulations of the cyclic voltammograms where performed using DigiSim.[38] The irreversible peak potentials were corrected to $E_{1/2}$ values by assuming that the disproportionation in eq 4 has a similar rate constant to the dimerization observed for $\mathbf{S_4Me}^{\bullet}$ (see Supporting Information for more details). Correcting the observed irreversible peak potentials at each scan rate and concentration results in average $E_{1/2}$ values of -0.91 ± 0.05 and -1.24 ± 0.05 V for the $\mathbf{S_4H}^{+/\bullet}$ and $\mathbf{S_4H}^{\bullet/-}$ couples, respectively. As is true for the $\mathbf{S_4Me}^{+/\bullet}$ and $\mathbf{S_4Me}^{\bullet/-}$ couples discussed in the preceding paragraph, any errors in the estimation of the true potentials of the individual $\mathbf{S_4H}^{+/\bullet}$ and $\mathbf{S_4H}^{\bullet/-}$ couples will not affect thermochemical data that require both values, as the errors will be equal and opposite and therefore cancel out when both of the potentials are used.

Finally, electrochemical studies of $\mathbf{S_4}$ indicate that this complex undergoes a reversible oxidation at -0.17 ± 0.02 V and a reversible reduction at -1.65 ± 0.02 V. These couples are reversible over a large range of scan rates (0.05−5 V/s). The electrochemical data described in this section, as well as data determined previously for related complexes, are summarized in Table 1.

Construction of Thermodynamic Schemes. The pK_a values and redox potentials described in the preceding section can be used in thermodynamic cycles to calculate a number of additional thermodynamic parameters. These parameters can then be used to construct thermodynamic schemes such as the one shown in Scheme 1 for the $\mathbf{S_4MeH}$ system. As discussed above, knowledge of the pK_a value measured for $\mathbf{S_4MeH_2}^+$, the potential of the $\mathbf{S_4MeH}^{+/o}$ couple, and a common thermodynamic cycle[39,40] can be used to determine the homolytic SBDFE

Scheme 1. Experimental Thermochemical Data for $\mathbf{S_4MeH}_x$ in Acetonitrile, Showing the Relationships between $E_{1/2}$, pK_a, Homolytic SBDFE, and ΔG_H. Values[a]

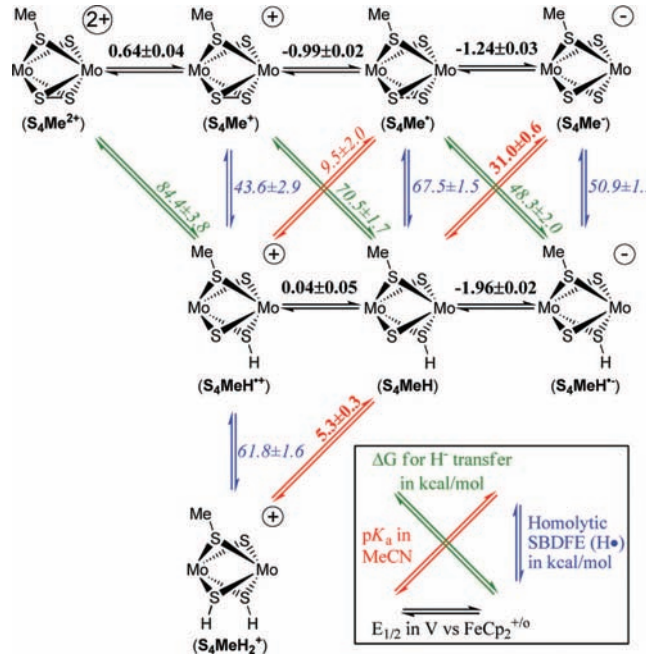

[a] Bold values are directly measured (all $E_{1/2}$ and two pK_a values), whereas values in italics are determined using the measured values and thermodynamic cycles.

of 61.8 kcal/mol for $\mathbf{S_4MeH_2}^+$ (see eqs 5−9, below, for a similar cycle). In Scheme 1 these three reactions, deprotonation of $\mathbf{S_4MeH_2}^+$ (red diagonal arrows), oxidation of the resulting $\mathbf{S_4MeH}$ complex (horizontal black arrows), and the homolytic cleavage of the S−H bond of $\mathbf{S_4MeH_2}^+$ (blue arrows) form three sides of a triangle. If the values of any two sides are known, then the third can be calculated. This simple idea can be used to build up more extensive themodynamic diagrams such as the one shown in Scheme 1.

Scheme 1 is a matrix of three rows and four columns of related chemical species. Upon moving from the top row to the bottom row, the number of hydrogen atoms bound to different sulfur ligands increases from zero to two. That is, all the species in a row have the same number of hydrogen atoms. Similarly, each column contains species with the same charge, decreasing from +2 in the first column to −1 in the last column. As a result, horizontal (black) arrows represent reductions on moving from left to right, vertical arrows (blue) represent homolytic bond cleavage reactions moving from bottom to top, diagonal arrows moving up and to the right (red) are proton transfer reactions, and diagonal arrows moving up and to the left (green) are hydride transfer reactions. Redox potentials are expressed in volts versus $FeCp_2^{+/o}$, acidities in pK_a units, and homolytic SBDFEs and hydride donor abilities in kcal/mol.

The pK_a value and reduction potential of $\mathbf{S_4MeH}$ form two sides of a triangle on the right side of Scheme 1. By combining the pK_a value for $\mathbf{S_4MeH}$ (eq 5), the $\mathbf{S_4MeH}^{o/-}$ reduction potential (written as an oxidation in eq 6),[32] and the free energy for the reduction of a proton in acetonitrile (eq 7),[39,40] the homolytic SBDFE values in kcal/mol for $\mathbf{S_4MeH}^{\bullet-}$ dissociating

(38) Rudolph, M.; Feldberg, S. W. *DigiSim, 3.03b (CV)*; Bioanalytical Systems: West Lafayette, IN, 2004.
(39) Wayner, D. D. M.; Parker, V. D. *Acc. Chem. Res.* **1993**, *26*, 287–294.
(40) Ellis, W. W.; Raebiger, J. W.; Curtis, C. J.; Bruno, J. W.; DuBois, D. L. *J. Am. Chem. Soc.* **2004**, *126*, 2738–2743, see Supporting Information.

to $\mathbf{S_4Me}^-$ and a hydrogen atom (eq 8) can be calculated using eq 9 (the sum of the free energies for eqs 5−7). For $\mathbf{S_4MeH}^{\bullet-}$, eq 9 gives a homolytic SBDFE value of 50.9 ± 1.3 kcal/mol. Using a similar thermodynamic cycle, the pK_a value of $\mathbf{S_4MeH}$ and the potential of the $\mathbf{S_4Me}^{\bullet/-}$ couple can be used to determine the homolytic SBDFE of $\mathbf{S_4MeH}$ (67.5 ± 1.5 kcal/mol) and complete another triangle in the overall thermodynamic scheme. By repeating this process using various thermodynamic cycles, all of the remaining thermodynamic values shown in Scheme 1 can be determined (see Supporting Information for details of the other cycles used). Due to error propagation, the SBDFEs on the left side of Scheme 1 have larger uncertainties than those on the right.

$$\mathbf{S_4MeH} \rightleftharpoons \mathbf{S_4Me}^- + H^+ \quad pK_a \tag{5}$$

$$\mathbf{S_4MeH}^{\bullet-} \rightleftharpoons \mathbf{S_4MeH} + e^- \quad -E_{1/2} \tag{6}$$

$$H^+ + e^- \rightleftharpoons H^\bullet \quad E_{1/2} \tag{7}$$

$$\mathbf{S_4MeH}^{\bullet-} \rightleftharpoons \mathbf{S_4Me}^- + H^\bullet \quad \text{homolytic SBDFE} \tag{8}$$

$$\text{SBDFE} = (1.37 \times pK_a) + (23.06 \times E_{1/2}) + 53.6 \tag{9}$$

A similar approach was used to determine the thermodynamic values shown in Scheme 2 for $\mathbf{S_4H_3}^+$. Because $\mathbf{S_4H_3}^+$ contains three S−H bonds, there are now four rows in this scheme corresponding to species containing 0−3 hydrogen atoms.

Combining all of the determined thermochemical data for $\mathbf{S_4H_n}^{+/o/-}$ ($n = 0-3$) results in a total of seven homolytic SBDFE values, five pK_a values, and four free energies for hydride transfer in addition to the electrochemical potentials. The overall similarity of the data in Schemes 1 and 2 provides additional confidence that the thermodynamic values are reasonable and internally consistent.

Discussion

Free Energy Landscapes for S−H Bonds. Due to the wealth of thermochemical data, the relative free energies of the species in Schemes 1 and 2 can be difficult to envision. One approach to simplifying the visualization of the thermochemical data is to convert Schemes 1 and 2 into a format in which the relative energies of the species are presented using three-dimensional free energy landscapes (also called free energy maps) as shown in Figures 2 and 3. The primary advantage that free energy landscapes have is the ease of comparison of the relative free energies for multiple species under varying conditions of pH and H_2 pressure. For example, a catalytic cycle for the reduction of protons to H_2 will involve a minimum of three species, but more likely four or five. Understanding the relative energetics of the catalytic intermediates can help to both optimize the conditions for a specific catalyst and lead to the development of improved catalysts by understanding which intermediates are high in energy in a catalytic cycle.

Free energy landscapes can be constructed by calculating the relative free energies of the species in the thermochemical schemes, as described below. The layout for the base of each graph (x and y axes) is the same as for Schemes 1 and 2, wherein the number of S−H bonds decreases from front to back ($\mathbf{S_4MeH_2}$ to $\mathbf{S_4Me}$ or $\mathbf{S_4H_3}$ to $\mathbf{S_4}$) and the charge decreases from left to right ($\mathbf{S_4MeH_x}^{2+}$ to $\mathbf{S_4MeH_x}^-$ or $\mathbf{S_4H_x}^+$ to $\mathbf{S_4H_x}^-$). The vertical axis, or z axis, has been added, and the height of each bar represents the free energies of the species relative to the most stable species under the conditions specified (i.e., pH 5 and 1.0 atm of H_2 in acetonitrile, under which conditions $\mathbf{S_4MeH_2}^+$ is the most stable and therefore set to 0 kcal/mol). All of the reactions shown in Schemes 1 and 2 involve two $\mathbf{S_4Me_xH_y}$ species, which differ by either an electron or H^+, $H^\bullet$,

Scheme 2. Experimental Thermochemical Data for $\mathbf{S_4H_x}$ in Acetonitrile, Showing the Relationships between $E_{1/2}$, pK_a, Homolytic SBDFE, and $\Delta G_{H^\bullet}$ Values[a]

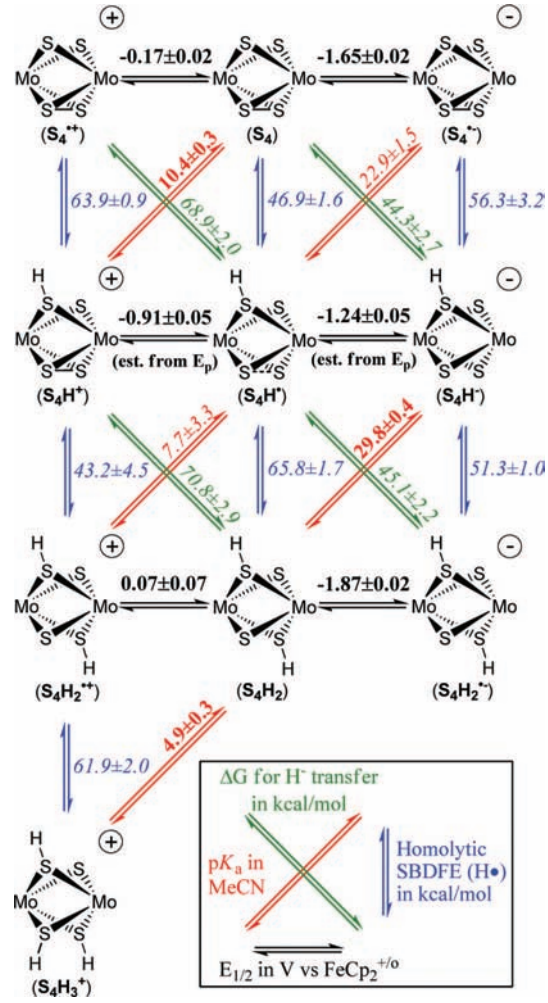

[a] Bold values are directly measured (all $E_{1/2}$ and three pK_a values) and values in italics are determined using thermochemical cycles.

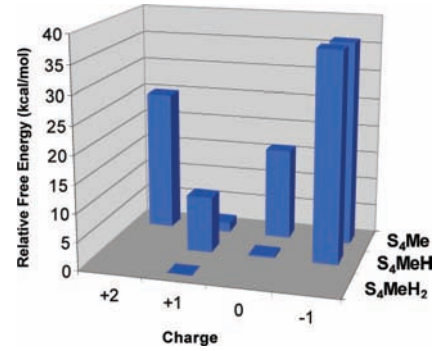

Figure 2. Free energy landscape for $\mathbf{S_4MeH_n}$ at pH 5 and 1.0 atm of H_2 in acetonitrile, showing the relative free energies of $\mathbf{S_4MeH_2}$, $\mathbf{S_4MeH}$, and $\mathbf{S_4Me}$ species from front to back and the dicationic, cationic, neutral, and anionic species from left to right.

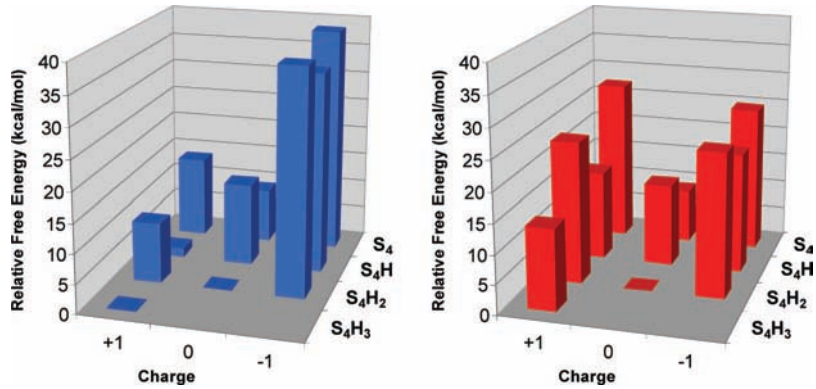

Figure 3. Free energy landscape for $\mathbf{S_4H_n}$ at 1.0 atm of H_2 and pH 5 (in blue on the left) or 15 (in red on the right) in acetonitrile, showing the relative free energies of $\mathbf{S_4H_3}$, $\mathbf{S_4H_2}$, $\mathbf{S_4H}$, and $\mathbf{S_4}$ species from front to back and the cationic, neutral, and anionic species from left to right.

or H^-. In order to determine the relative free energies of the two $\mathbf{S_4Me_xH_y}$ species, the free energy for transferring H^+, $H^\bullet$, or H^- or an electron to or from protons or H_2 in solution has to be defined. This can be done by expressing the free energy for transferring H^+, $H^\bullet$, or H^- or an electron in terms of the solution pH and pressure of hydrogen. In the case of electron transfer, the free energy can be expressed relative to the potential of the hydrogen electrode in acetonitrile, which is defined by the solution pH and pressure of hydrogen. While the hydrogen electrode in acetonitrile has a specific potential under standard conditions (−0.07 V vs $FeCp_2^{+/o}$),[40] most reactions and catalysis are not performed at pH 0 and 1.0 atm of H_2. Therefore, free energy landscapes may have greater utility under nonstandard conditions. In order to convert Schemes 1 and 2 to nonstandard conditions, the effects of changing the solution pH and pressure of H_2 must be considered.

The simplest relative free energies to determine are those for species separated by a proton transfer, such as $\mathbf{S_4H_3}^+$ to $\mathbf{S_4H_2}$. The relative free energy between the two species is defined by eq 10.

$$\mathbf{S_4H_3^+} \rightleftharpoons \mathbf{S_4H_2} + H^+_{(MeCN)} \qquad 1.37 \times (pK_a - pH) \tag{10}$$

At pH 0, the relative free energies of the two species simplifies to $1.37 \times pK_a$, or 6.7 kcal/mol for this example, given the pK_a of 4.9 for $\mathbf{S_4H_3}^+$. However, moving to pH 5 will result in a much smaller free energy difference between the two species, as the pH and the pK_a are essentially the same, as illustrated on the left side (blue graph) in Figure 3.

The pressure of hydrogen will affect hydrogen atom transfer reactions. The extent of the effect can be quantified using eqs 11−13, where $\mathbf{S_4H^\bullet}$ and $\mathbf{S_4H_2}$ are used as the example:

$$\mathbf{S_4H^\bullet} + H^\bullet_{(MeCN)} \rightleftharpoons \mathbf{S_4H_2} \quad -SBDFE \tag{11}$$

$$^1/_2H_{2(g)} \rightleftharpoons H^\bullet_{(MeCN)} \quad 51.8 - 1.37 \times \log(P^{1/2}_{H2}) \tag{12}$$

$$\mathbf{S_4H^\bullet} + {}^1/_2H_{2(g)} \rightleftharpoons \mathbf{S_4H_2} \quad -SBDFE + 51.8 - 1.37 \times \log(P^{1/2}_{H2}) \tag{13}$$

Equation 12 includes both the SBDFE for dissociation of H_2 at standard state (51.8 kcal/mol)[39] and the effect of changing the pressure of hydrogen. Similar expressions can be developed to account for the effects of pH and hydrogen pressure on the relative stabilities of additional species, as discussed in more detail in the Supporting Information. Combining changes in pH and pressure of hydrogen, the free energy landscapes are capable of providing extensive insight into the relative free energies of all relevant species, as demonstrated in the interactive spreadsheet in the Supporting Information.

Once constructed, the free energy landscapes can help to explain many of the reactions that occur for these complexes. For example, addition of H_2 to $\mathbf{S_4}$ to form $\mathbf{S_4H_2}$ is predicted to be 9 kcal/mol downhill using Figure 3 (at either pH), consistent with the experimental observation that H_2 addition occurs at 1.0 atm, quantitatively converting $\mathbf{S_4}$ to $\mathbf{S_4H_2}$. Species that are expected to disproportionate can be identified using the free energy landscape merely by checking the relative heights of the bars surrounding the species of interest. One example is $\mathbf{S_4H^\bullet}$ in Figure 3, where disproportionation to $\mathbf{S_4}$ and $\mathbf{S_4H_2}$ is expected (eq 4, above), and has been observed for the analogous complex, $CpMo(\mu\text{-}S_3)(\mu\text{-}SH)MoCp$.[23] The sum of the relative free energies of $\mathbf{S_4}$ and $\mathbf{S_4H_2}$ is less than twice that for $\mathbf{S_4H^\bullet}$, thereby indicating that two $\mathbf{S_4H^\bullet}$ are less stable than one $\mathbf{S_4}$ and one $\mathbf{S_4H_2}$. Similarly, while cyclic voltammograms of the oxidation of $\mathbf{S_4Me_2}$ to form $\mathbf{S_4Me_2}^{\bullet+}$ are completely reversible at all scan rates,[32] the oxidation of $\mathbf{S_4MeH}$ or $\mathbf{S_4H_2}$ to form either $\mathbf{S_4MeH}^{\bullet+}$ or $\mathbf{S_4H_2}^{\bullet+}$ are found to be irreversible at slow scan rates, consistent with disproportionation to form either $\mathbf{S_4Me}^+$ and $\mathbf{S_4MeH_2}^+$ or $\mathbf{S_4H}^+$ and $\mathbf{S_4H_3}^+$. Changing from $\mathbf{S_4Me_2}$ to $\mathbf{S_4MeH}$ or $\mathbf{S_4H_2}$ allows for the disproportionation of $\mathbf{S_4MeH}^{\bullet+}$ or $\mathbf{S_4H_2}^{\bullet+}$ to form two more stable species, as shown in Figures 2 and 3.

While the free energy landscapes are useful for visualizing the relative free energies of the many species shown under one set of conditions, they are also helpful for comparing the relative free energies of the same species under different conditions. One example is shown in Figure 3, where the pH is changed from 5 to 15, significantly altering the relative stabilities of the species. At pH 5, $\mathbf{S_4H_3}^+$ and $\mathbf{S_4H_2}$ have nearly the same energy and are also close in energy to $\mathbf{S_4H}^+$, whereas at pH 15, $\mathbf{S_4H_2}$ is still the lowest in energy, but free energies of $\mathbf{S_4H_3}^+$ and $\mathbf{S_4H}^+$ have increased by about 14 kcal/mol. Figure 3 is just one example showing the effects of a change in pH upon the relative free energies.

In addition to the above examples of relatively simple reactions involving two or three species, possible catalytic cycles can also be considered. Figure 4 contains a free energy landscape at pH 5.3 for five of the $\mathbf{S_4MeH_\textit{n}}$ species which could comprise a catalytic cycle for hydrogen oxidation. This would start with the addition of hydrogen to $\mathbf{S_4Me}^+$ to form $\mathbf{S_4MeH_2}^+$ (−1.7

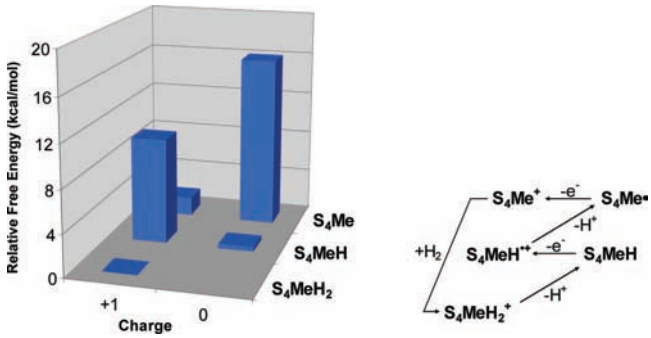

Figure 4. On the left, free energy landscape for $\mathbf{S_4Me}_n$ at 1.0 atm of H_2 and pH 5.3 in acetonitrile, showing the relative free energies of $\mathbf{S_4MeH_2}^+$, $\mathbf{S_4MeH}^{+/o}$, and $\mathbf{S_4Me}^{+/\bullet}$ species. On the right, possible cycle for hydrogen oxidation.

Table 2. Solution Homolytic and Heterolytic S−H Bond Dissociation Free Energies for $\mathbf{S_4Me}_x\mathbf{H}_y$ Complexes in Acetonitrile[a]

complex	pK_a	SBDFE (kcal/mol)	ΔG_{H^-} (kcal/mol)
$\mathbf{S_4H}^+$	**10.4 ± 0.3**	**63.9 ± 0.9**	
$\mathbf{S_4H}^\bullet$	22.9 ± 1.5	46.9 ± 1.6	68.9 ± 2.0
$\mathbf{S_4H}^-$		56.3 ± 3.2	44.3 ± 2.7
$\mathbf{S_4H_2}^{\bullet+}$	7.7 ± 3.3	43.2 ± 4.5	
$\mathbf{S_4MeH}^{\bullet+}$	8.4 ± 2.1	43.7 ± 3.6	84.5 ± 4.5
$\mathbf{S_4H_2}$	**29.8 ± 0.4**	65.8 ± 1.7	70.8 ± 2.9
$\mathbf{S_4MeH}$	31.0 ± 0.6	66.1 ± 1.7	70.6 ± 2.5
$\mathbf{S_4H_2}^{\bullet-}$		51.3 ± 1.0	45.1 ± 2.2
$\mathbf{S_4MeH}^{\bullet-}$		50.9 ± 1.3	46.9 ± 2.0
$\mathbf{S_4H_3}^+$	**4.9 ± 0.3**[b]	61.9 ± 2.0[b]	
$\mathbf{S_4MeH_2}^+$	**5.3 ± 0.3**[b]	61.8 ± 1.6[b]	
$\mathbf{S_4Me_2H}^+$	**5.6 ± 0.4**[b]	60.8 ± 1.0[b]	

[a] Directly measured values are in bold. [b] Data for $\mathbf{S_4H_3}^+$, $\mathbf{S_4MeH_2}^+$, and $\mathbf{S_4Me_2H}^+$ from Appel, et al.[32]

kcal/mol), followed by deprotonation to **S$_4$MeH** (0.0 kcal/mol), oxidation to form $\mathbf{S_4MeH}^+$ (+10.0 kcal/mol), deprotonation to $\mathbf{S_4Me}^\bullet$ (+5.7 kcal/mol), and finally oxidation to reform $\mathbf{S_4Me}^+$ (−14.0 kcal/mol). While some of the steps are nearly thermoneutral, the oxidation of **S$_4$MeH** to $\mathbf{S_4MeH}^+$ and the subsequent deprotonation to form $\mathbf{S_4Me}^\bullet$ are not. The oxidation of **S$_4$MeH** to $\mathbf{S_4MeH}^+$ alone would result in an overpotential of more than 400 mV. One approach to decreasing this energy mismatch is to couple a following downhill reaction to the uphill steps, as has been previously described.[41] The use of free energy diagrams to study catalytic cycles allows the energies of all involved intermediates to be visualized and therefore can focus efforts to improve catalytic activity by pinpointing energy mismatches, such as the ones shown in Figure 4.

Comparison of the MS−H Bond Thermochemistry. The thermochemical data for the S−H bonds in the dinuclear molybdenum sulfide complexes, summarized in Table 2, cover a much broader range of values than those of the S−H bonds in organic thiols. In addition, the data show remarkable breadth for an isostructural series of metal complexes in which no alteration of metal ion or ligating atoms is involved. In general, the pK_a and $\Delta G°_{H^-}$ values follow trends that one would expect on the basis of electronic contributions from substituents and charge effects. For example the pK_a values increase and the $\Delta G°_{H^-}$ values decrease as the overall charge on the complex becomes more negative. However, within this general framework, some interesting comparisons can be made. The ligand protonation reaction (eq 14) and the one-electron oxidation of the neutral complex **S$_4$H$_2$** (eq 15) lead to two distinct cationic products; the data permit a quantitative comparison on how each of these reactions affects the expected decrease in pK_a.

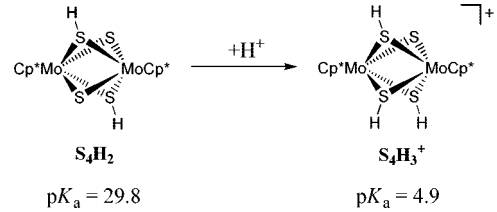

(14)

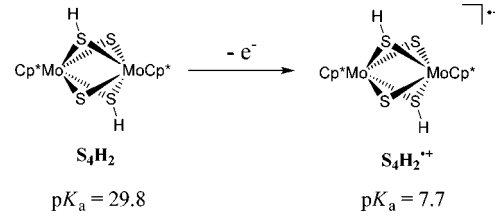

(15)

In the conversion of $\mathbf{S_4H}^+$ to $\mathbf{S_4H_3}^+$ (eq 16), a formal addition of dihydrogen to a disulfide bond occurs, and neither the overall charge on the complex nor the formal oxidation states of the molybdenum ions change. Nevertheless, the conversion results in a significant decrease in the pK_a value of the respective S−H ligands. A similar consequence might be expected to occur when hydrogen is added to molybdenum sulfide surfaces.

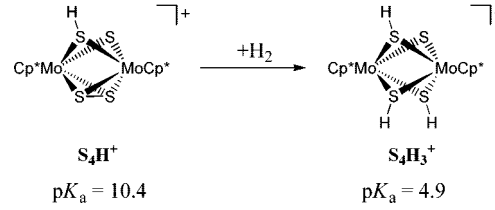

(16)

The hydride donor abilities of S−H ligands have not been determined previously for any metal complexes. As expected, the anionic complexes ($\mathbf{S_4H}^-$, $\mathbf{S_4H_2}^{\bullet-}$, and $\mathbf{S_4MeH}^{\bullet-}$) are the best hydride donors of the series with $\Delta G°_{H^-}$ values of 44−48 kcal/mol. It is somewhat surprising that these values are comparable to those of relatively strong hydride donors within other classes of compounds. For example the hydridic reducing agent $NaBH_3(CN)$ is estimated to have a $\Delta G°_{H^-}$ value of ca. 45 kcal/mol,[42,43] while in the metal hydride series of the formula HM(diphosphine)$_2$, $\Delta G°_{H^-}$ values for HCo(dppe)$_2$ = 49 kcal/mol, for $[HPt(dmpp)_2]^+$ = 51 kcal/mol, and for $[HPt(depe)_2]^+$ = 44 kcal/mol.[33,44] These complexes have been used as hydride donors to a variety of metal carbonyl complexes to form the corresponding formyl complexes.[45,46] At the other extreme, the hydride acceptor ability of $\mathbf{S_4Me}^{2+}$ (−84 kcal/mol) is comparable to that of the $[p\text{-}(CH_3OC_6H_4)_3C]^+$ carbenium ion (−86 kcal/mol).[47]

Unlike the other thermodynamic data, the solution S−H bond dissociation free energies do not vary in a systematic way with

(41) DuBois, M. R.; DuBois, D. L. *Chem. Soc. Rev.* **2009**, *38*, 62–72.
(42) Arnett, E. M.; Flowers, R. A.; Ludwig, R. T.; Meekhof, A. E.; Walek, S. A. *J. Phys. Org. Chem.* **1997**, *10*, 499–513.
(43) Price, A. J.; Ciancanelli, R.; Noll, B. C.; Curtis, C. J.; DuBois, D. L.; DuBois, M. R. *Organometallics* **2002**, *21*, 4833–4839.
(44) Curtis, C. J.; Miedaner, A.; Ellis, W. W.; DuBois, D. L. *J. Am. Chem. Soc.* **2002**, *124*, 1918–1925.
(45) Miedaner, A.; DuBois, D. L.; Curtis, C. J.; Haltiwanger, R. C. *Organometallics* **1993**, *12*, 299–303.
(46) Ellis, W. W.; Miedaner, A.; Curtis, C. J.; Gibson, D. H.; DuBois, D. L. *J. Am. Chem. Soc.* **2002**, *124*, 1926–1932.

the charge of the complexes. The entire range of values, which varies from ca. 66 to 43 kcal/mol, is lower than the range observed for organic thiols (reported $\Delta H° = 79-92$ kcal/mol,[48,49] which corresponds to a $\Delta G°$ of 74−87 kcal/mol),[39] reflecting the electronic influence of the metal ions on the S−H bond strengths. The lower S−H bond energies of these molybdenum dimers compared to organic thiols undoubtedly contribute to the facile hydrogen atom transfer reactions observed for certain hydrosulfido complexes of molybdenum dimers which have been found to be useful in synthetic and catalytic applications.[9,21] Additionally, the decrease in S−H bond strengths resulting from metal coordination to the sulfides and hydrosulfides produces S−H bonds that are similar to M−H bonds.[50−52]

In this series of molybdenum sulfide complexes, the S−H bond dissociation free energies are >56 kcal/mol for diamagnetic, or closed shell, complexes which become paramagnetic upon loss of a hydrogen atom, while conversions from open to closed shell species, e.g., $\mathbf{S_4H_2}^{\bullet+} \rightarrow \mathbf{S_4H}^+$ and $\mathbf{S_4H_2}^{\bullet-} \rightarrow \mathbf{S_4H}^-$, involve significantly lower energies in the range of 43−51 kcal/mol. This trend in bond strengths is similar to closed and open shell transition metal hydride complexes.[33] In general, the homolytic and heterolytic SBDFEs of these molydenum sulfide complexes are comparable to those of transition metal hydrides, revealing the underlying thermodynamic basis that results in the ability of these molybdenum sulfur dimers to undergo many of the same transformations that have been traditionally associated with transition metal hydrides, including electrocatalytic hydrogen production[6] and hydrogen activation for hydrogenation and hydrogenolysis reactions.[7−11]

The similarities between S−H and M−H bonds are remarkable, even though the H^+, $H^\bullet$, and H^- based reactivity in molybdenum sulfides complexes does not appear to involve M−H bonds. The homolytic and heterolytic S−H bond strengths obtained give prototypical guidance to the reactivity observed for heterogeneous molybdenum sulfide catalysts and suggest that the reactions observed for heterogeneous metal sulfide catalysts occur at sulfur rather than directly at the metal centers. The determined S−H bond strengths provide the first models of hydrogen atom reactivity (surface to substrate H transfer, free H atom production, proton transfer, hydride transfer) on heterogeneous MoS catalysts for important categories of reactive intermediates: highly acidic centers, highly basic centers, highly destabilized and reactive S−H functional groups, radical anion, radical cation and neutral S−H donors. The current bond strengths allow prediction of expected half-lives for bimolecular transfer of hydrogen to aromatic and olefinic organic acceptors (e.g., molecular disproportionation pathway).

Conclusions

An extensive and complete thermochemical understanding of S−H bonds in homogeneoues molybdenum sulfide complexes has been developed. The range of determined homolytic and heterolytic bond strengths are similar to those observed for transition metal hydride complexes, consistent with the similarities in reactivities between metal hydrides and metal hydrosulfides. The current thermochemical data can serve as a basis for the validation of subsequent computational efforts and as a model for heterogeneous molybdenum sulfide catalysts, for which analogous data cannot be obtained.

Free energy landscapes have been developed, and these landscapes have been shown to help identify and visualize the relative free energies of multiple species under varying conditions of pH and H_2 pressure. Understanding the relative free energies of complexes in multiple oxidation states and with different numbers of bonds to hydrogen will help not only for the prediction of equilibria in simple reactions, but also for the identification of high energy intermediates in catalytic cycles. As shown in the present work, homolytic and heterolytic bond strengths vary substantially with the redox state of the complex. Thermochemical information such as in this work exemplifies the control over bond strengths that can be achieved using electrochemistry, and how solution conditions can be optimized for specific reactions of interest. This control is essential for the development of highly effective and energy efficient catalysts and electrocatalysts that will be needed as the demand for energy production, storage, and utilization continues to increase.

Experimental Procedures

Instrumentation. ^{1}H NMR spectra were acquired using a Varian Inova 500 or VXR-300 spectrometer, and the chemical shifts were referenced to the residual solvent peak at (1.94 ppm for acetonitrile-d_3). Electrochemical data were collected using a CH Instruments model 660C computer-aided three-electrode potentiostat in acetonitrile with 0.3 M tetraethylammonium tetrafluoroborate. For cyclic voltammetry the working electrode was a glassy carbon disk, the counter electrode was a glassy carbon rod, and a silver chloride-coated silver wire was used as a pseudo-reference electrode and was separated from the main compartment by a Vycor disk (1/8 in. diameter) obtained from Bioanalytical Systems, Inc. Ferrocene or decamethylferrocene was used as an internal reference with all potentials reported versus the $FeCp_2^{+/o}$ couple. CV simulations were run using DigiSim.[38]

Materials. Reagents were purchased commercially and used without further purification unless otherwise specified. All reactions, syntheses, and manipulations of Mo_2S_4 complexes were carried out under nitrogen using standard Schlenk techniques or in a glovebox. Acetonitrile and THF were dried by activated alumina column in an Innovative Technology, Inc., PureSolv system or by distillation from calcium hydride (acetonitrile) or sodium and benzophenone (THF). CD_3CN was dried over activated sieves, degassed, and stored in a glovebox. Potassium *t*-butoxide, *p*-bromoaniline, and *p*-anisidine were purified by vacuum sublimation and stored in a glovebox. Molybdenum complexes $\mathbf{S_4H_2}$,[13] $\mathbf{S_4}$,[24,53] $\mathbf{S_4Me}^+$,[24] $\mathbf{S_4MeH}$,[24] and $\mathbf{S_4Me_2}$[32] were prepared as previously reported.

Isolation of Protonated Bases. Tetrafluoroboric acid (54% in diethyl ether, 1.0 mL, 7.3 mmol) was added to *tert*-butyliminotri(pyrrolidino)phosphorane (BTPP, 1.5 g, 4.9 mmol) in 120 mL of diethyl ether. The resulting precipitate was collected by filtration, washed with 100 mL of diethyl ether, and dried under vacuum to give 1.8 g of solid (93% yield). The tetrafluoroborate salts of *p*-bromoaniline and *p*-anisidine were isolated by similar procedures.

Equilibrium Measurements. All measurements were made at 22 ± 3 °C. The pK_a values were determined by NMR and were measured for three or more independent samples. The electrochemical potentials are the average of the measured $E_{1/2}$ values for reversible couples over scan rates of 0.05−50 V/s where applicable. The reported errors in the acid/base equilibria included two standard deviations for the reproducibility plus an additional 0.2 pK_a units

(47) Zhang, X. M.; Bruno, J. W.; Enyinnaya, E. *J. Org. Chem.* **1998**, *63*, 4671–4678.
(48) Bordwell, F. G.; Zhang, X.-M.; Satish, A. V.; Cheng, J. P. *J. Am. Chem. Soc.* **1994**, *116*, 6605–6610.
(49) Benson, S. W. *Chem. Rev.* **1978**, *78*, 23–35.
(50) Simoes, J. A. M.; Beauchamp, J. L. *Chem. Rev.* **1990**, *90*, 629–688.
(51) Sherry, A. E.; Wayland, B. B. *J. Am. Chem. Soc.* **1990**, *112*, 1259–1261.
(52) Wayland, B. B.; Ba, S.; Sherry, A. E. *J. Am. Chem. Soc.* **1991**, *113*, 5305–5311.
(53) Brunner, H.; Meier, W.; Wachter, J.; Guggolz, E.; Zahn, T.; Ziegler, M. L. *Organometallics* **1982**, *1*, 1107–1113.

to allow for uncertainty in the pK_a values of the reference bases. Similarly, the reported errors in electrochemical potentials are two standard deviations for the reproducibility plus an additional 10 mV to account for any errors in the potentials of the references.

pK_a Determinations. The pK_a values for $\mathbf{S_4Me_2H^+}$, $\mathbf{S_4MeH_2^+}$, and $\mathbf{S_4H_3^+}$ have been previously reported,[32] and the values for the protonated aniline derivatives and BTPP were taken from the self-consistent scale published by Kaljurand, et al.[36] The pK_a values for the Mo_2S_4 complexes were determined against known bases using ^{1}H NMR at analyte and reference concentrations <25 mM. The observed acid−base equilibria using the aniline derivatives, BTPP, and the Mo_2S_4 complexes gave average peaks resulting from rapid exchange of protons between the base and acid forms of each species. The weighted averages of the shifts were used to determine the ratio of acid to base forms of each species. These ratios were then used to determine the equilibrium constant for eq 1, and thereafter the pK_a of the analyte in eq 2. The determined pK_a values for the Mo_2S_4 complexes are listed in Table 2. Each value is the average of four or more measurements and include verifications of reversibility. For example, an equilibrium was measured between BTPP and $\mathbf{S_4H_2}$, and then protonated BTPP was added, shifting the equilibrium away from $\mathbf{S_4H^-}$ and back toward $\mathbf{S_4H_2}$, and the equilibrium was remeasured in order to verify that $\mathbf{S_4H_2}$ deprotonated reversibly.

The pK_a for $\mathbf{S_4H^+}$ was determined starting from $\mathbf{S_4}$ and either *p*-bromoaniline or *p*-anisidine and the corresponding tetrafluoroborate salt. The pK_a of $\mathbf{S_4H_2}$ and $\mathbf{S_4MeH}$ were each determined by this procedure using BTPP and its tetrafluoroborate salt. The two pK_a values were checked against each other by making solutions of approximately 1:1:1 $\mathbf{S_4MeH}$, $\mathbf{S_4H_2}$, and potassium *t*-butoxide to partially deprotonate the Mo_2S_4 complexes. Additionally, the pK_a of $\mathbf{S_4MeH}$ was measured with 2,8,9-trimethyl-2,5,8,9-tetraaza-1-phosphabicyclo[3.3.3]undecane (Verkade superbase, pK_a = 32.90);[37] however, in this case the reference base and its conjugate acid did not interconvert rapidly on the NMR time scale, and so the relative integrated areas were used to determine the ratio of base and protonated base for the reference.

Cyclic Voltammetry. Data for the $\mathbf{S_4Me_2}^{\bullet+/o/\bullet-}$, $\mathbf{S_4MeH}^{\bullet+/o/\bullet-}$, and $\mathbf{S_4H_2}^{\bullet+/o/\bullet-}$ couples have been previously reported.[32] Data for the $\mathbf{S_4Me^{2+/+/\bullet/-}}$, $\mathbf{S_4H^{+/\bullet/-}}$, and $\mathbf{S_4}^{\bullet+/o/\bullet-}$ couples are shown in Table 1 and Schemes 1 and 2. The $\mathbf{S_4H^{+/\bullet/-}}$ waves were completely irreversible; thus, the data were corrected for the second-order disproportionation assuming the same rate constant determined previously for the dimerization of $\mathbf{S_4Me^\bullet}$ (6.3×10^7 M^{-1} s^{-1}).[24] Corrections for each scan rate and concentration were determined using DigiSim,[38] and details of these corrections are included in the Supporting Information. Uncorrected peak potentials are shown in Table 1, and the corresponding estimates of $E_{1/2}$ are in Scheme 2.

Acknowledgement. This work was supported by the U.S. Department of Energy's (DOE) Office of Basic Energy Sciences, Chemical Sciences program. The Pacific Northwest National Laboratory is operated by Battelle for DOE.

Supporting Information Available: An interactive spreadsheet demonstrating the pH and H_2 pressure dependence of the free energy landscapes for $\mathbf{S_4MeH_x}$ and $\mathbf{S_4H_x}$, as well as details of the CV simulations, an example of the pK_a determinations, and additional details of the cycles used to determine the thermochemical data. This material is available free of charge via the Internet at http://pubs.acs.org.

JA8093179